Fractals, Vol. 3, No. 1 (1995) 33–53

FRACTAL TRACER PATTERNS IN OPEN HYDRODYNAMICAL FLOWS: THE CASE OF LEAPFROGGING VORTEX PAIRS

Á. PÉNTEK*, T. TÉL, and Z. TOROCZKAI†
Institute for Theoretical Physics, Eötvös University,
Puskin u. 5–7, H–1088, Budapest, Hungary

Received December 19, 1994, Accepted December 25, 1994

Abstract

Patterns obtained by using tracer particles to visualize open hydrodynamical flows are investigated. As an example, the advection problem of passive tracers in the time-periodic velocity field of leapfrogging vortex pairs is considered. We show that the patterns are fractal if the tracer dynamics is chaotic, i.e., there exists a chaotic saddle, and if the initial conditions overlap with the stable manifold of this chaotic set (that is itself a fractal). Dye particles not advected away very quickly then accumulate on the unstable manifold of the chaotic saddle and the fractal dimension of such patterns is thus independent of the initial conditions. The time evolution of the fractal patterns appearing on snaphsots is followed within one period of the velocity field. We investigate which features of the chaotic dynamics determine the fractal properties. They turn out to be independent of when the snapshots are taken. The entropy function of the local Lyapunov exponents is computed based on the scattering motion of the tracer particles, along with the $f(\alpha)$ spectrum of the chaotic saddle.

*Present address: Institute for Pure and Applied Physical Sciences, University of California at San Diego, La Jolla, California 92093-0075, USA
†Present address: Department of Physics, Virginia Polytechnic Institute and State University, Blacksburg, Virginia 24061, USA

1. INTRODUCTION

Fractal patterns can often be seen in open hydrodynamical flows with the naked eye. In this paper we concentrate on patterns traced out by ensembles (e.g., droplets) of dye particles. These passive tracers are assumed to have negligible inertia and the same density as the fluid, so that they simply follow the local velocity field.[1,2,3] An interesting observation is that turbulence is *not* a necessary condition for the existence of fractal structures; the latter can appear in any *nonstationary* flow with smooth instantaneous streamlines. *Time-periodic* cases provide the simplest class with potential fractal patterns. To understand this we recall that streamlines and particle trajectories coincide in stationary flows only.[1] In the presence of any time-dependence they can drastically differ since particles have to follow a streamline pattern changing continuously with time. Our aim is to find conditions for the fractality of tracer patterns. We shall show that the *chaotic motion* of the particles is the origin of such patterns and investigate which features of the chaotic dynamics determine the fractal behavior.

As an illustrative example we consider a simplified model of the so-called *leapfrogging* motion of two vortex rings. With some experience, smokers can make such rings. Having the same sense of rotation, these rings travel in the same direction. In cases where they happen to move along the same axis, the rear vortex ring attempts to pass through the front one. The leading ring then widens due to mutual interaction and slows down. Simultaneously, the other ring shrinks, travels faster and penetrates the first one. The process is then repeated again and again. A detailed simulation of particle trajectories in the field of leapfrogging vortex rings in viscid fluid has been carried out recently,[4,5] and good agreement with smoke visualization pictures reported in experiments[6] has been found. For further experiments with vortices see Ref. 7. We shall study the two-dimensional analogue of this process in an inviscid incompressible flow: advection by two pairs of ideal point vortices of the same strength exhibiting leapfrogging motion and generating a time periodic velocity field.

The analysis of this problem requires a dynamical system approach and also leads to the description of the emerging fractal patterns. The main results from the point of view of dynamical system theory have been summarized in Ref. 8. Here, we concentrate on the fractal aspects without giving too much mathematical details. Instead, we can also discuss numerical results that have not been presented in Ref. 8, for example, the different ways of approaching the fractal pattern, the time dependence of the latter within one period of the velocity field, and multifractal properties.

The paper is organized as follows. In Sec. 2 we qualitatively describe the motion of leapfrogging vortices and the associated advection problem (the equations of motion are given in the Appendix). Results of numerical experiments are presented showing how dye droplets of different shapes approach the same fractal pattern. A more detailed description of the process is provided by plotting in different color tracers injected into the flow in front of the vortex system during different full periods of the velocity field. We shall see that the so-called invariant set of the tracer dynamics discussed in Sec. 3 play a fundamental role in understanding the advection of tracer ensembles. Bounded trajectories corresponding to tracer particles trapped forever by the vortex system form a nonattracting chaotic set, a *chaotic saddle* for short. This set is a fractal, of measure zero, resembling the direct product of two Cantor sets. It has a *stable manifold*, a foliation of the fluid in front of the vortices along which the chaotic saddle can be reached. Since this foliation is also a fractal of measure zero there is no finite probability for tracer particles to reach the chaotic saddle and to be trapped forever among the vortices. The chaotic saddle also has an unstable manifold, the stable manifold of the time reversed tracer dynamics. We point out that *fractal patterns of the tracer dynamics coincide with the unstable manifold* of the chaotic saddle. The time evolution of the invariant sets is followed numerically on snapshots taken within one period of the velocity field. Afterwards (Sec. 4) we study the mixing and transport properties and show how the motion of the manifolds' lobes, the so-called lobe dynamics, determine the time spent around the vortices and the stretching and folding of material lines. Finally (Sec. 5), the escaping process and the multifractal properties of the chaotic saddle are discussed. The paper concludes with an extension of the results to general open flows and a brief discussion of potential experimental implications.

2. NUMERICAL RESULTS FOR THE TRACER DYNAMICS

The description of tracer dynamics implies the solution of two types of problems: first the

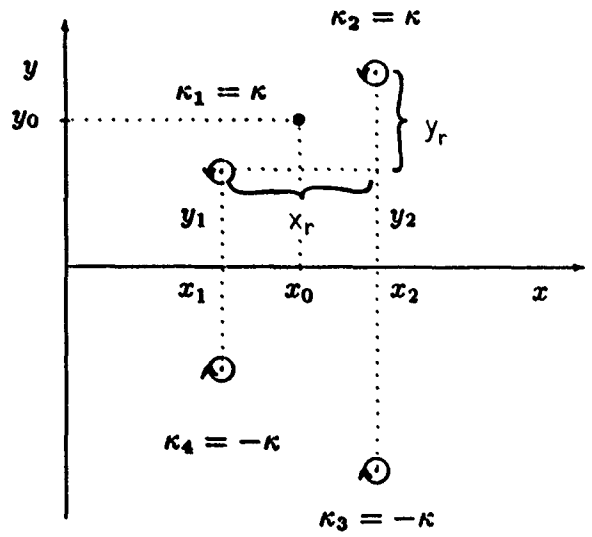

Fig. 1 Geometry of two leapfrogging vortex pairs. Relative and center of mass coordinates are indicated.

determination of the velocity field, and then the solution for the tracer trajectories in this field.

An isolated point vortex of strength κ generates at distance r from its center a circulational flow with a velocity field proportional in modulus to κ/r.[10] In an n-vortex system, each vortex is simply advected by the flow induced by the others, i.e., the velocity of a given vortex is the vectorial sum of the velocities generated at its position by the $n-1$ other vortices. We consider the situation depicted in Fig. 1 corresponding to the motion of two vortex pairs of equal strength ($\kappa_1 = \kappa_2 = -\kappa_3 = -\kappa_4 = 1$) that move in the same direction along a common symmetry axis perpendicular to the extension of both pairs ($x_1 = x_4$, $y_1 = -y_4$, $x_2 = x_3$, $y_2 = -y_3$). It is easy to write down the equations of motion of these vortices, and since the symmetry with respect to the x axis is assumed to hold during the motion, only vortices 1 and 2 are independent. These equations turn out to be integrable by simple quadratures and possess strictly periodic solutions describing a leapfrogging motion. We set the origin of time $t = 0$ so that it corresponds to a configuration when the upper two vortices have the same y-coordinate.

Using the law describing the velocity around a given vortex, it is also easy to determine the velocity field $\mathbf{v}$ at any point $\mathbf{r} \equiv (x, y)$ of the plane. This velocity is, however, explicitly time dependent because the vortex centers move as determined above.

A passive tracer particle located at $\mathbf{r}$ at time t simply follows the local velocity field $\mathbf{v}$ of the flow; therefore, its equation of motion is:

$$\dot{\mathbf{r}} = \mathbf{v}(\mathbf{r}, t). \tag{1}$$

This is a set of nonautonomous ordinary differential equations containing $\mathbf{v}$, the result of the vortex dynamics, as an input. In the case of leapfrogging, the velocity is time periodic with some period T. The advection problem is then similar to the dynamics of driven nonlinear oscillators that are known to be chaotic in general.[11] The phenomenon is especially simple in a frame comoving with the center of mass $x_0 \equiv (x_1 + x_2)/2$ of the upper two vortices, and all the numerical results will be given in a reference frame whose origin is at $(x_0(t), 0)$.

We have numerically solved Eq. (1) with several initial conditions to find tracer trajectories $\mathbf{r}(t)$. Because of the periodicity of the velocity field, it is convenient to represent the results by taking snapshots of the tracer positions at integer multiples of the period T. This defines a so-called *stroboscopic map* of the tracer dynamics that we shall extensively use in what follows.

In this section we present results obtained with ensembles of tracer particles injected in front of the vortex system into the flow. In Fig. 2 we take a droplet of circular shape close to the x axis, and follow it while it is being transported by the flow. One can clearly see that the droplet is very strongly stretched and after one period (Fig. 2(b)) it is already so narrow that it cannot be distinguished from a line segment. This line is then elongated and deformed further. After three periods (Fig. 2(c)) a part of this segment has flown out of the range shown but its other part stays inside. This segment becomes longer and longer and seems to trace out a complicated pattern surrounding the upper two vortices. Because of the symmetry of the vortex problem, tracer particles can never cross the x axis. However, if we had initiated a droplet on the lower half plane at the mirror image position of what is shown in Fig. 2(a), we would have obtained the mirror images of Figs. 2(b)–2(f) with respect to the x axis. Figure 2 is taken at $t = 0 \bmod T$ and the vortex centers are located at $x = \pm 0.5$, $y = 0.5$. Note that the tracer particles do not penetrate the immediate vicinity of the vortex centers.

Figure 3 shows an analogous series of pictures obtained with another ensemble of tracer particles now distributed along a horizontal straight line segment $2 \leq x \leq 3.96$, $y = 0.1$. Although the first 3 steps are rather different, the part of this material line that remains for long around the vortices seems

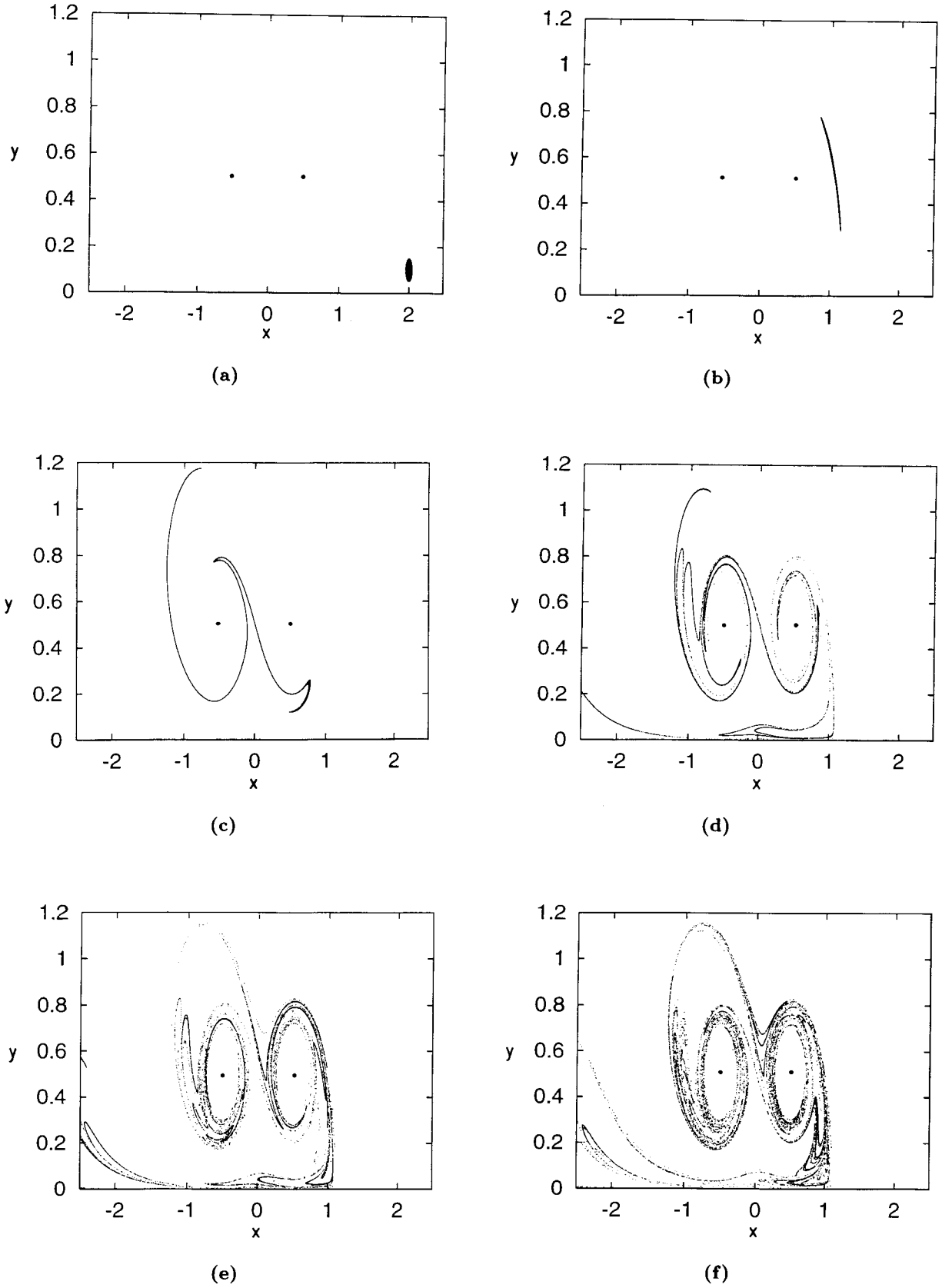

Fig. 2 Motion of a droplet of dye particles on the upper half of the stroboscopic plane taken at $t = nT$ with n an integer between 0 and 5 **(a–f)**. $5 \cdot 10^4$ tracer particles were started from a disc of radius 0.05 centered at $(2, 0.1)$. Observe that after only five time steps the ensemble of dye particles converges to a fractal pattern. The vortex centers are denoted by dots.

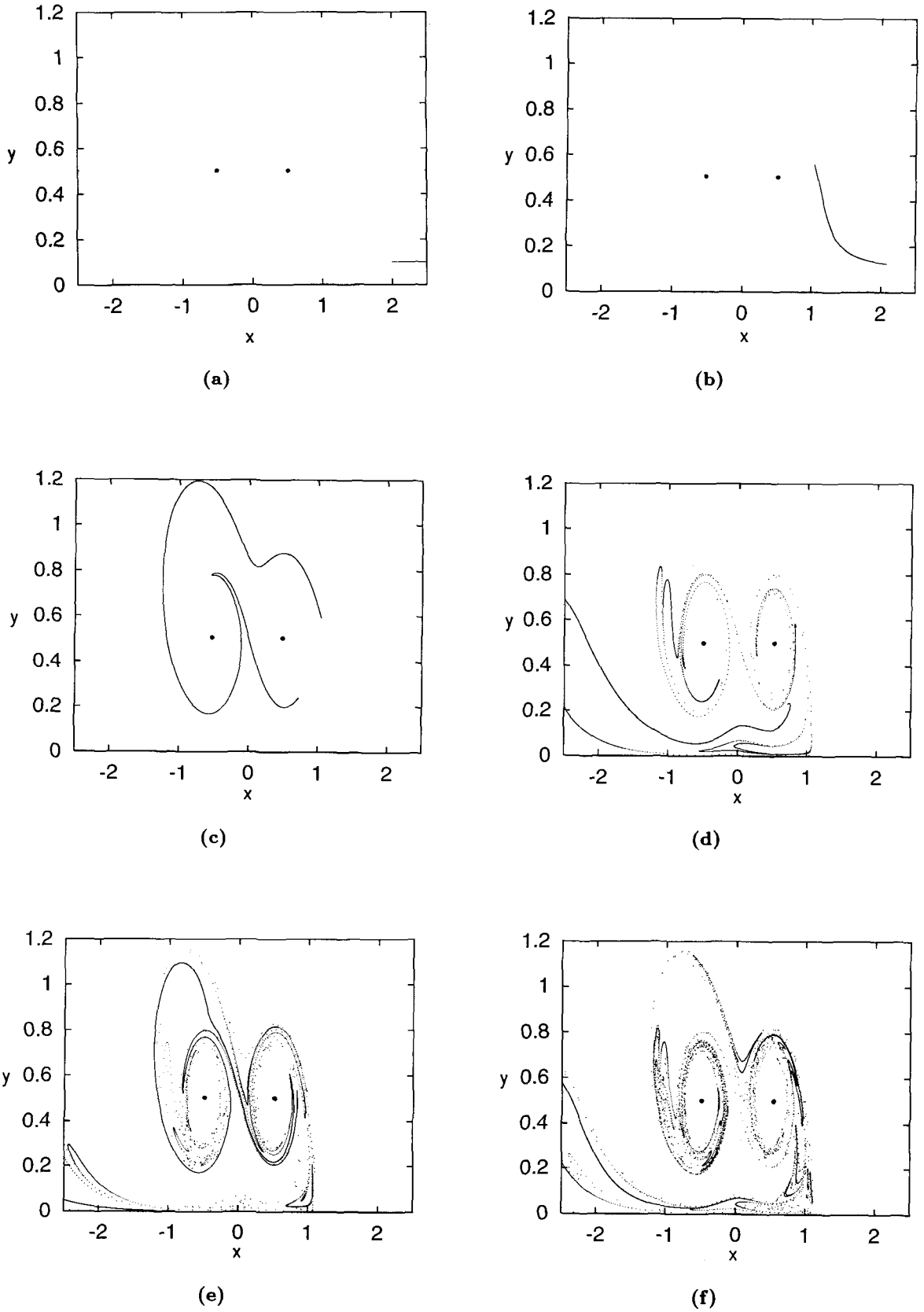

Fig. 3 Motion of a material line on the stroboscopic plane taken at $t = nT$ with $n = 0, \ldots, 5$ **(a–f)**. $5 \cdot 10^4$ evenly distributed tracer particles were started from a horizontal straight line segment $\{2 \leq x \leq 3.96,\ y = 0.1\}$. The ensemble of dye particles traces out asymptotically the same pattern as in Fig. 2(f). The vortex centers are denoted by dots.

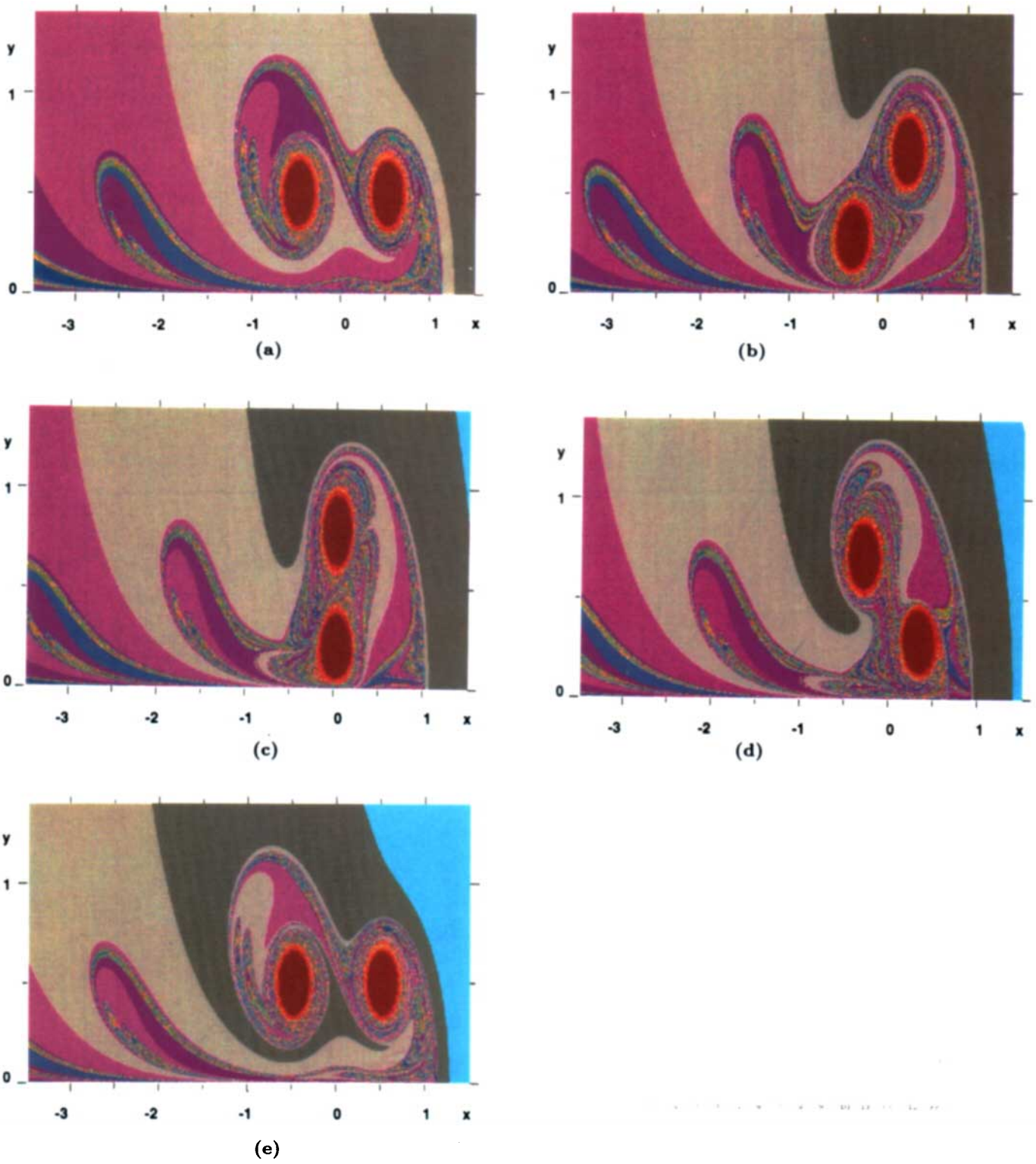

Fig. 4 Motion in a fluid whose color is changing. Dye particles are injected along the vertical line $x = 4$. The color is changed after each full time period T. The index used in the legend of color coding indicates the color of tracers injected in the period $(n-1)T \leq t \leq nT$. Light red marks tracers injected more than 12 periods before. The red regions corresponds to the vortex cores not reachable by tracers coming from outside, and can formally be considered as regions of infinite lifetimes. Part **(a)** displays the distribution of differently colored tracers at $t_0 = 99\ T$. (Numerically it has been convenient to obtain it by starting trajectories on a grid of 800×400 points in the range shown, iterating the tracer dynamics backward, and coloring the initial points according to the time the tracers needed to cross the $x = 4$ line.) Figs. b–e show how these material regions evolve in time by taking snapshots at $t - t_0 = 0.356\ T$, $0.5\ T$, $0.644\ T$, T. Note that Fig. 4(e) is the same as Fig. 4(a) but the color code has been shifted by 1.

to converge to the *same* pattern as the droplet of Fig. 2.

The white ellipsoidal regions around the vortices (see e.g. Figs. 2f and 3f) are obviously not accessible by incoming trajectories. These are the regions where the effect of one vortex dominates that of any other one and can therefore be called the *vortex core* for the tracer dynamics. Inside this core the other vortices produce just a weak perturbation of the rotational motion generated by the vortex in the center. Tracer particles injected directly into this regime can therefore have simple trajectories.

A more detailed description of the convergence toward a complicated pattern can be obtained by introducing *color coding* according to the time spent in the vicinity of the vortex system. Figure 4(a) exhibits the result of a numerical experiment in which particles have been injected into the flow along the vertical line $x = 4$, $y > 0$ continuously but by changing the color of the dye after each full period T: a domain of color $(n + 1)$ is the image of the domain of color (n) under the stroboscopic map. The boundary between domains of different colors is thus the image of the material line $x = 4$, $y > 0$ after a certain multiple of T. Notice that the boundary between different colors converges in certain regions to a curve. An example is the curve crossing the x axis approximately perpendicularly around $x = 1.1$ and appearing as the left boundary of the light gray domain. Although here all the colors have to accumulate, the convergence is so fast that not even light magenta can be seen on the picture. In the next section we shall see that this curve is a well defined mathematical object, the unstable manifold of a periodic orbit. That a layer of light magenta is present around this curve becomes clear by considering the upper left loop where the convergence is slower. In other regions, for example, in the loops behind the vortices, no sign of convergence can be observed; a broad light magenta band is present.

Another point of interest is that the light magenta domain (the image of the light gray one) penetrates from two directions, the surrounding of the vortices, which we shall call the interaction region (see Sec. 4). A narrow filament very close to the x axis enters this region and broadens considerably forming patches, for example left above the left vortex and around $x = 0$, $y = 0.05$. The other light magenta band comes in above the first loop behind the vortices and surrounds the multicolored region with a single layer that is quite broad below the right and above the left vortex but nearly invisible at other places. These observations illustrates the fact that while the bulk of the domain of a given color is transported away, filaments of it remain trapped around the vortices. The thickness of these filaments is decreases greatly with time: yellow and blue is much less dominating around the vortices than magenta. Despite their complex forms, each domain of a given color forms a *single connection* domain. Note that in certain regions, for example, between the vortices and around the x axis, an efficient stretching takes place: the dark magenta filament is very narrow and hardly visible, respectively, in these regions. Parallel to this there is a continuous escape of the tracers that have ever entered into the interaction region and, consequently, *no finite amount* of matter will be trapped by the vortex system *forever*. There is however, *a finite portion* of tracers that is trapped *for a long time*, and it is this amount of matter that will be strongly *mixed* and *transported* away by the vortices.

It can also clearly be observed that particles with long lifetimes between the vortices (from blue to light red) trace out the same pattern as that of Figs. 3(f) and 4(f). The longest lifetimes can be found around the outer surface of the vortex cores. Their insides, formally of infinite lifetimes, are colored by red.

The series of pictures 4(b)–4(e) shows how domains of different colors evolve during a full period. It nicely illustrates that some parts of the compact light gray domain of Fig. 4(a) are stretched and rolled up between the vortices. Some other parts are transported simply to infinity or are just smoothly deformed. The huge light gray domain below the vortices in Fig. 4(a) appears to be cut from the rest of the light gray domain in Fig. 4(b) and transported further to the upper left lobe of Fig. 4(e). Similarly the thin light gray tongue in the middle of Fig. 4(a) seems to be cut from the rest in Fig. 4(b) and is shifted to the bottom light gray patch around $x = 0$, $y = 0.05$ of Fig. 4(e). *Stretching* and *folding* illustrated by these plots is known to be the basic mechanism for chaotic dynamics[11] and is responsible for the creation of fractal structures.

3. THE CHAOTIC SADDLE AND ITS STABLE AND UNSTABLE MANIFOLDS

The existence of sets that are invariant under the time evolution of maps plays an essential role in

the theory of dynamical systems. Such invariant sets are fixed points or other periodic orbits, chaotic sets, and their stable and unstable manifolds.[11]

The key observation in understanding the formation of fractal patterns by tracer ensembles is the existence of an *invariant chaotic saddle*[9] in the configuration space of the flow. The concept of a chaotic saddle is an extension of that of a saddle (or hyperbolic) point. Roughly speaking one can say that the former contains an infinity of saddle points corresponding to unstable periodic orbits. All the trajectories of the tracer dynamics that after a full period (or integer multiples of it) return exactly to their initial points belong to the set. Interestingly, the number of such trajectories increases with the period and the invariant set contains thus an infinity of points. This set is *globally* nonattracting and cannot be reached exactly. Particles, however, can come arbitrarily close to it and exhibit chaotic motion before escaping. The chaotic saddle is itself a *fractal* with a local structure resembling the direct product of two Cantor sets in certain regions (see the schematic Fig. 5).

There exists a powerful numerical method[12] to construct the chaotic saddle by finding a long sequence of short pieces of trajectories that straddle a true orbit on the set. The chaotic saddle plotted in this way is shown in Fig. 6. Only the upper half-plane is displayed since the full set is symmetric with respect to the x axis.

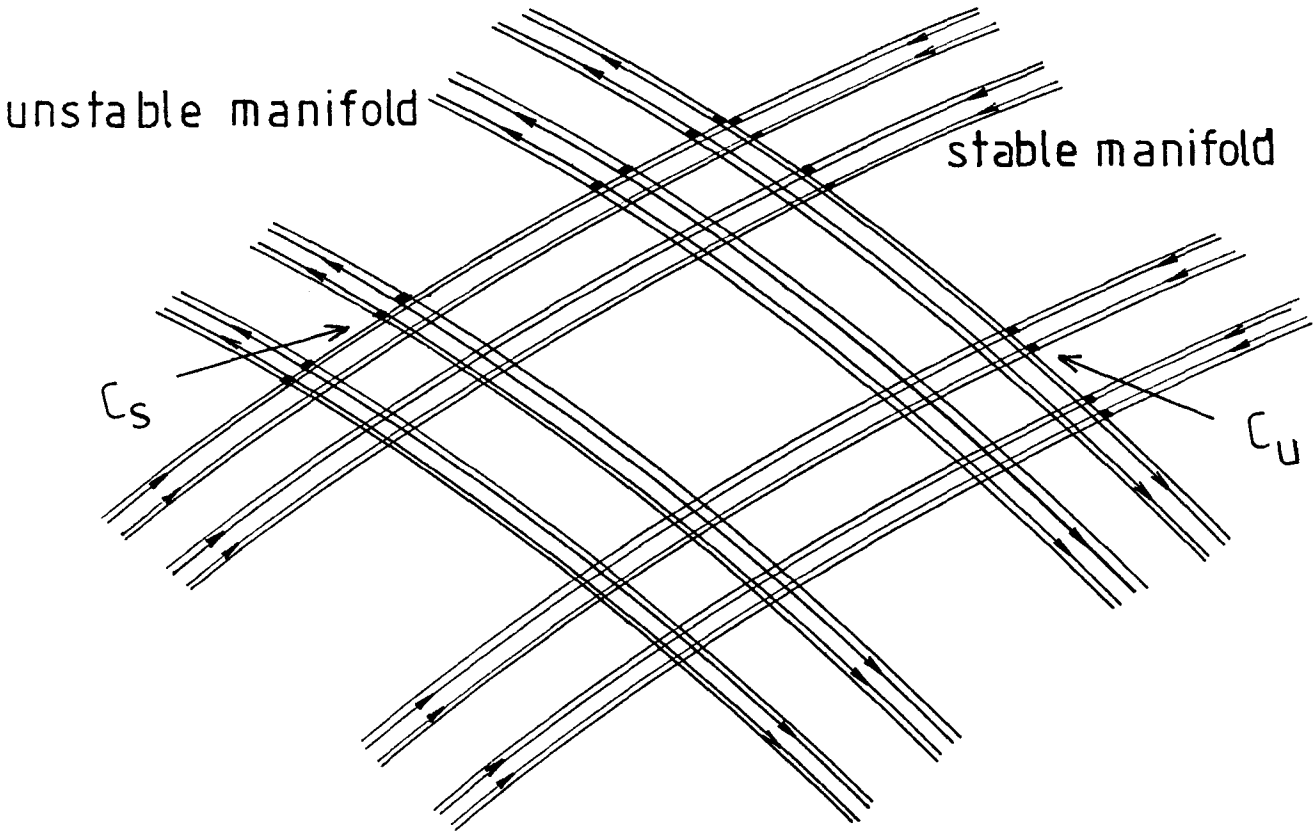

Fig. 5 Schematic diagram of the direct product structure of the chaotic set's hyperbolic component on the stroboscopic map. The building blocks, the Cantor sets C_s and C_u, are indicated.

The set can clearly be divided into two parts. One of them contains structures of double fractal character. The deltoidal form A along the y axis and structures B and C at the two sides of the plot of Fig. 6(a) taken at $t = 0$ (mod T) are of this type. Each of the two latter forms is mapped after a period T onto itself. The elongated structure D on the bottom of the figure and the deltoidal form A are images of each other after time T although the direct product structure of D is less striking because of the strong stretching along the x axis. These four blocks, that we shall call the *hyperbolic component*, contain the strongly unstable periodic orbits of the dynamics. It is worth noticing that two hyperbolic periodic orbits, P_1 and P_2 of period T, lie on the x axis (see Fig. 6(a)) and are the extremal points of the chaotic saddle. The hyperbolic component is equivalent to the direct product of two Cantor sets, $\mathcal{C}_s$ and $\mathcal{C}_u$ as depicted in Fig. 5. Because of the time reversal symmetry, both Cantor sets must have the same fractal dimension d_0. The hyperbolic component is thus of dimension $2d_0$. The other, the

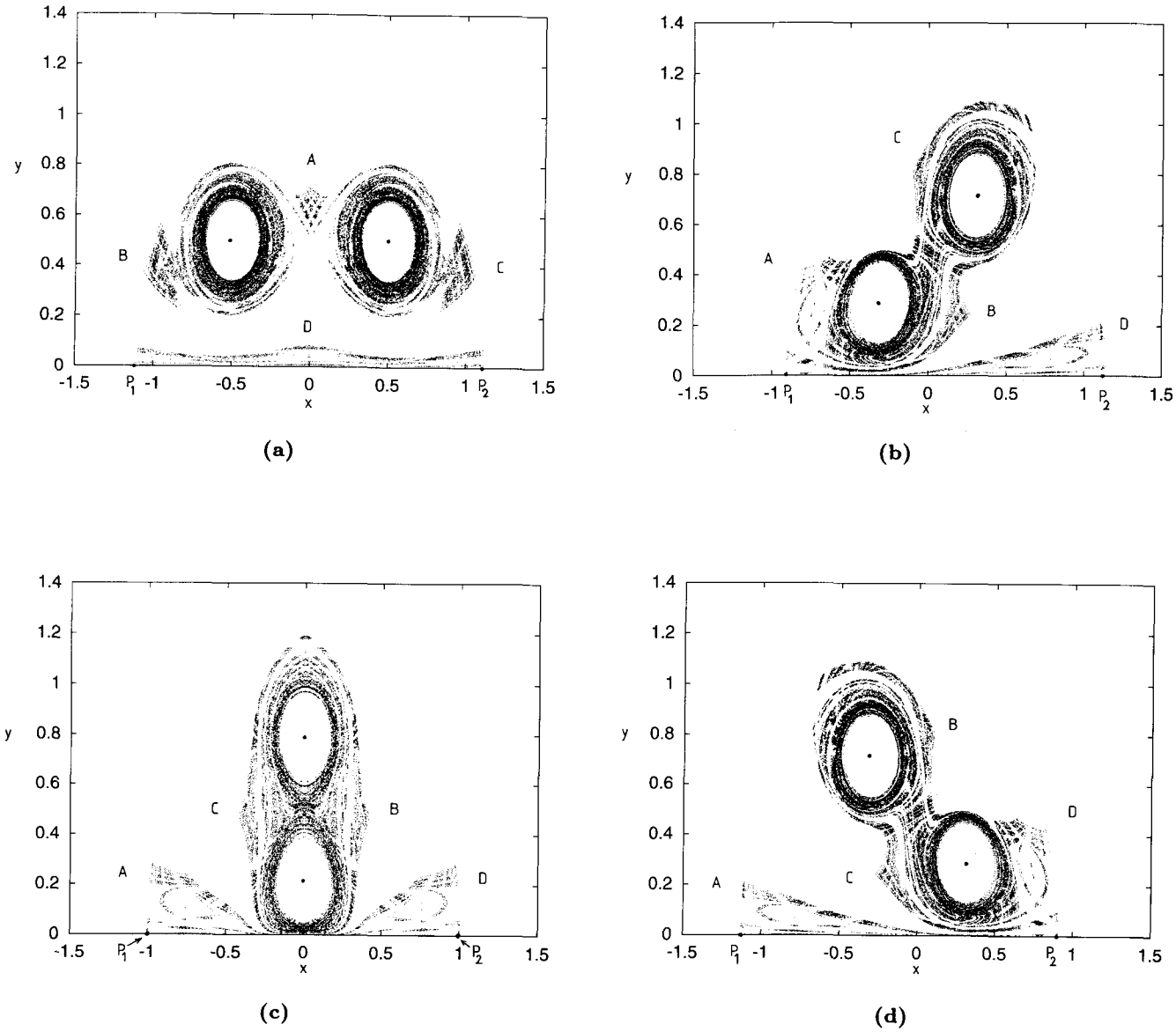

Fig. 6 The chaotic saddle at time $t = 0$, 0.356 T, 0.5 T, 0.644 T (mod T) on the upper half plane. Note the direct product structure of the hyperbolic part (see regions A, B, C, and D) and the dense spirals around the vortex cores forming the nonhyperbolic part. The vortex centers are denoted by dots.

nonhyperbolic, component is the dense part around the outer surface of the vortex cores where weakly unstable periodic orbits accumulate. On very fine scales this component appears to have fractal dimension 2 on the stroboscopic map.[13]

It is instructive to see how the chaotic saddle itself evolves in time during a full period (Figs. 6(b)–6(d)). By $t = 0.356\ T$ (Fig. 6(b)) the deltoidal form A becomes deformed and is transported to the left side of the lower vortex core. Simultaneously, structure D is pushed over to the positive half plane but still stays on the bottom of the picture. Form B (C) has been strongly stretched and rotated so that it is located now below and right (above and left) from the lower (upper) vortex core. Certain points come close to the midpoint between the two vortex centers. These components are deformed further so that after half a period (Fig. 6(c)) form A goes over into the left part of the "whiskers" on the bottom and its mirror image with respect to the y axis now coincides with structure D. The hyperbolic parts B and C are located on the right and left side of Fig. 6(c), respectively. The shape of the chaotic saddle at $t_2 = T - t_1$ is just the mirror image with respect to the y axis of that obtained at t_1.[8] Thus Fig. 6(d) belonging to time $t = 0.644\ T$ is the mirror image of Fig. 6(b) and helps to understand how the configuration of Fig. 6(a) will be restored again by $t = T$.

Just like an isolated hyperbolic point, a chaotic saddle also has a *stable manifold*, an invariant set of curves along which the set can be reached. It is essential that the stable manifold of a nonattracting chaotic set is an object of *measure zero* and provides a *fractal* foliation of the space. This is why a particle has zero probability to fall on the manifold and to be thus trapped forever by the chaotic saddle. Figure 7 displays the stable manifold of the chaotic saddle on the stroboscopic map taken at $t = 0 \bmod T$. One can show that the unstable manifold of the periodic point P_1 is a very good approximation to the stable manifold of the full chaotic saddle.

Tracer particles can approach the chaotic saddle only if their initial points lie close to a branch of the stable manifold. If this is not the case, like in the example shown in Fig. 8, the droplet will just

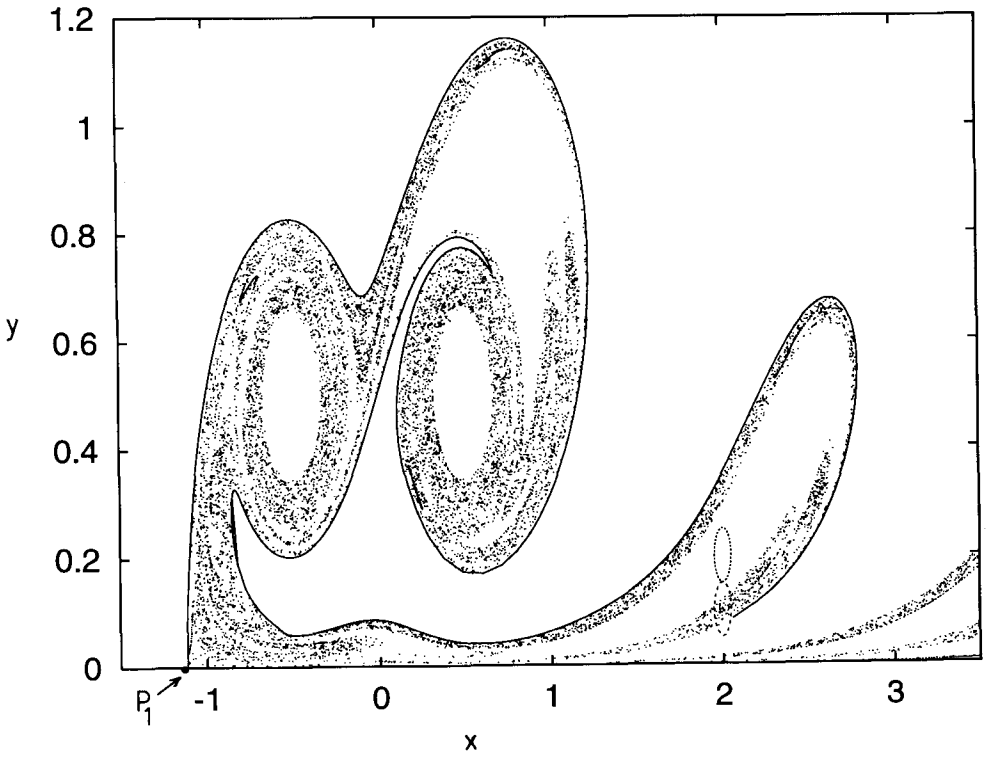

Fig. 7 The stable manifold of the chaotic saddle at $t = 0 \bmod T$. The droplets of initial conditions for Fig. 2 (dashed) and Fig. 8 (dotted) are also indicated. The manifold has been obtained by letting several particles start in a tiny semidisk around P_1 and following their time reversed tracer dynamics on the stroboscopic map.

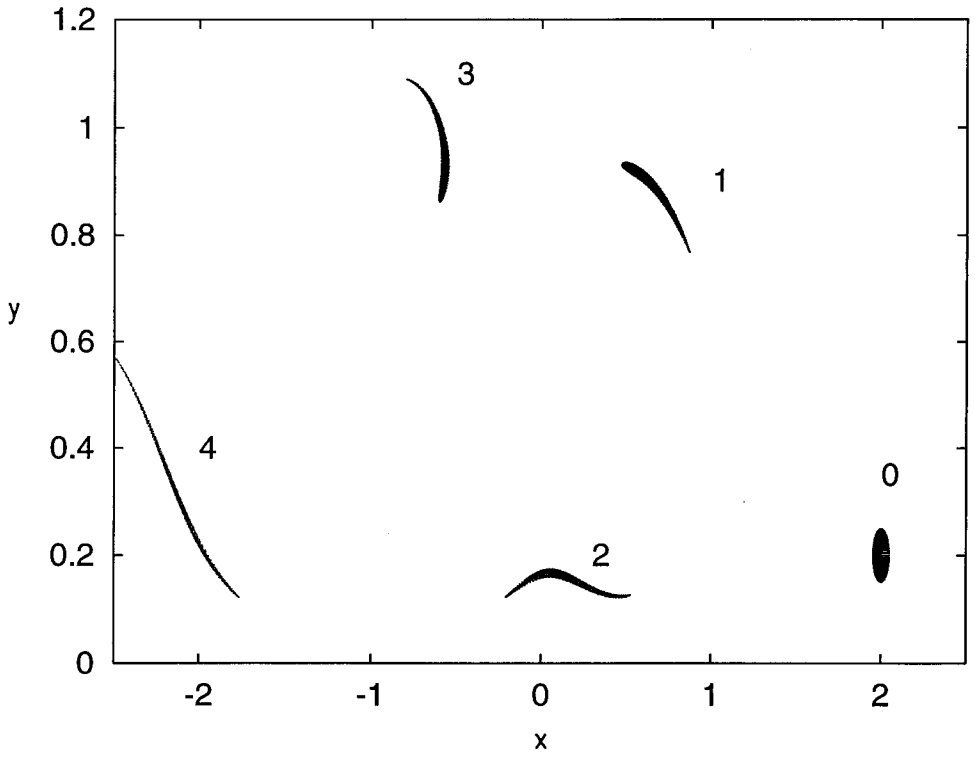

Fig. 8 Motion of a droplet of dye particles that initially do not overlap with the filaments of the chaotic saddle's stable manifold. Observe that the ensemble of particles is only smoothly deformed and is transported away rapidly. $5 \cdot 10^3$ tracer particles were started from a disc of radius 0.05 centered at $(2, 0.2)$.

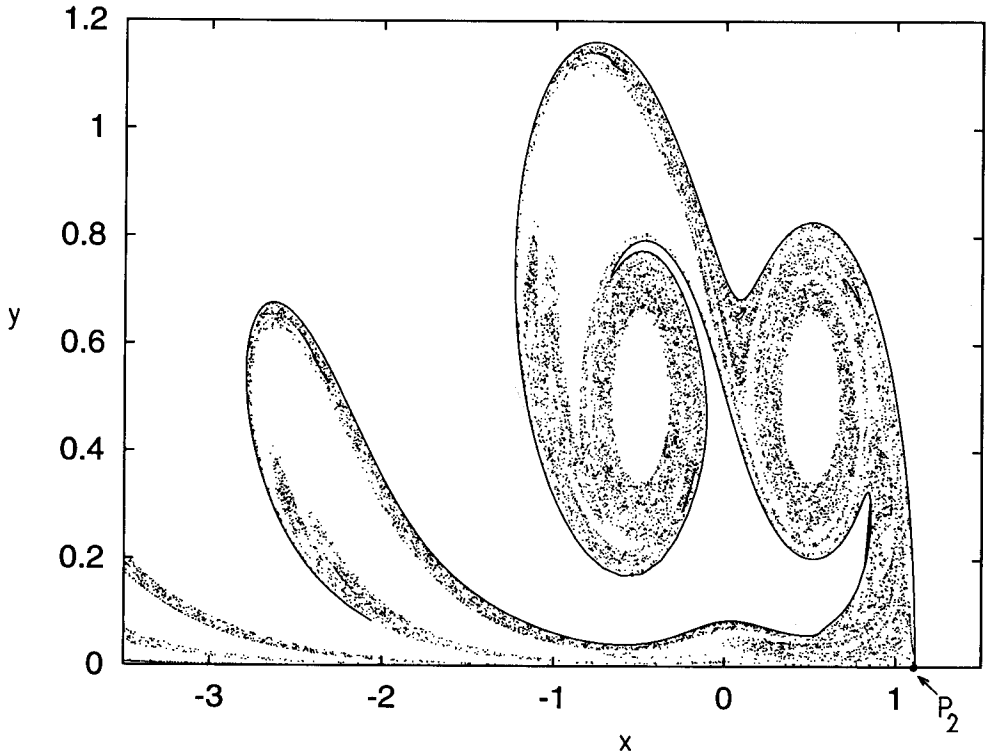

Fig. 9 The unstable manifold of the chaotic saddle at $t = 0 \pmod{T}$ obtained by letting several particles start in a tiny semidisk around P_2 and following their direct tracer dynamics on the stroboscopic map.

be deformed a little and then transported away by the flow. It is easy to check that the set of initial conditions used in Figs. 2–4 have indeed common parts with the stable manifold.

The chaotic saddle also has an *unstable manifold* that is a fractal, too, and can be defined as the stable manifold of the time reversed dynamics. This manifold is presented in Fig. 9 and is approximately the same as the unstable manifold of the periodic point P_2. Note that due to an internal symmetry of the problem, at $t = 0 \pmod T$ this is just the mirror image of the stable manifold taken with respect to the y axis. More generally, the unstable manifold at time t is the mirror image of the stable manifold at $(T - t) \bmod T$ taken with respect to the y axis.

The actual form of both manifolds is time-dependent but periodic with the same period as the flow. The manifolds on the stroboscopic map can be obtained as the direct products of a line and a Cantor set. Let $\mathcal{C}_u$ ($\mathcal{C}_s$) denote the Cantor set appearing as the intersection of the stable (unstable) manifold with one smooth branch of the unstable

Table 1 Hyperbolic Fractal Sets and Their Dimensions

Fractal Set	Dimension
Cantor sets $\mathcal{C}_s$, $\mathcal{C}_u$	d_0
Set of singularities in the time delay function	d_0
Saddle's hyperbolic component (stroboscopic map)	$2d_0$
Saddle's hyperbolic component (phase space of Eq. (1))	$2d_0 + 1$
Stable or unstable manifold (stroboscopic map)	$d_0 + 1$
Stable or unstable manifold (phase space of Eq. (1))	$d_0 + 2$

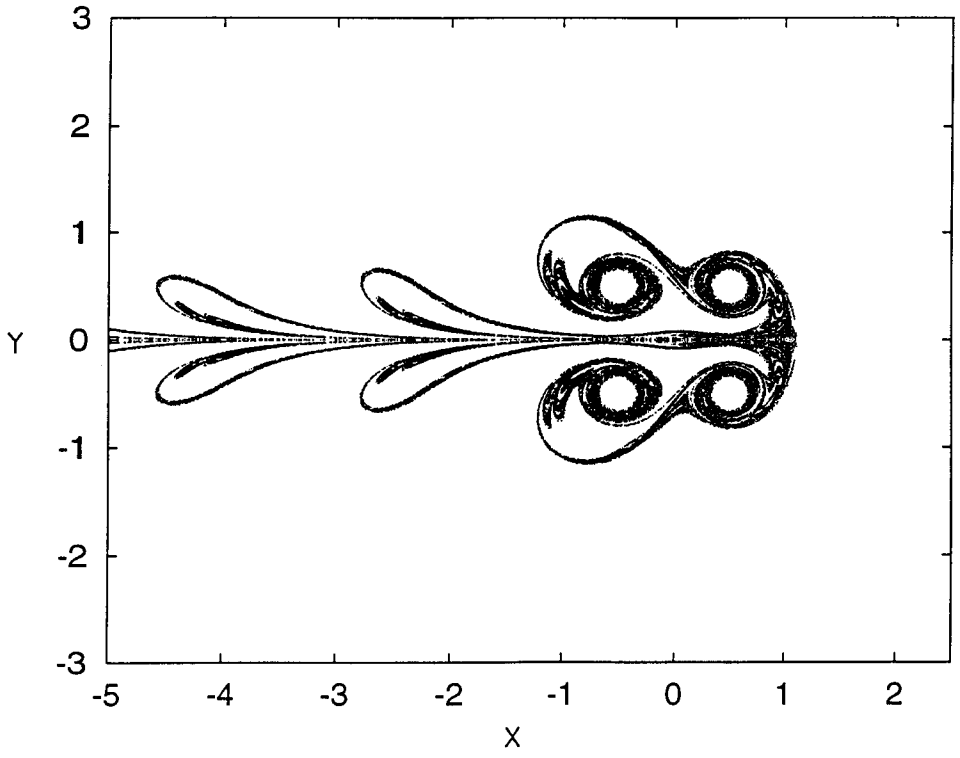

Fig. 10 Unstable manifold of the full chaotic saddle (the shape of the droplet of Fig. 2 at $t = 10\ T$ and its mirror image with respect the x axis) on large scale. It shows a similar form as the flow visualization pattern in an experiment with three-dimensional vortex rings.[6]

(stable) one in the hyperbolic part of the chaotic saddle (see Fig. 5). One thus concludes that the dimension of both manifolds is d_0+1 on any snapshot of the stroboscopic map. Since the trajectories are smooth curves in the time continuous dynamics, the manifolds are d_0+2 dimensional in the phase space of Eq. (1).

Fractal patterns observed in the tracer dynamics are attributed to the *double foliation* of the space by the two manifolds. If the initial points of the tracer trajectories lie close to one branch of the stable manifold, particles will approach the chaotic saddle along this branch, stay a relatively long time around the set, and finally escape along its unstable manifold. Thus, we conclude that dye particles not advected away quickly to the asymptotic region *lie close to the unstable manifold* of the chaotic saddle. A comparison of Figs. 2(f), 3(f) with Fig. 9 supports this observation. The approach to this manifold might strongly depend on the initial conditions used, for example on the shape of the droplet, but the final form is *independent*. Consequently, the fractal dimension of the tracer pattern is on any snapshot the same $d_0 + 1$ as that of the chaotic saddle's unstable manifold. In Table 1 we have collected the different fractal sets that play a role in the tracer dynamics and have nontrivial fractal dimensions.

It is also worth returning to the observations of Fig. 4 in view of the double foliation just discussed. Strips of different colors accumulate with a rapid convergence on a fractal curve, the unstable manifold, in a region around the chaotic saddle. Further away from this set, like for example, in the loops behind the vortices, the pattern at a given instant of time is just very slightly deformed and is transported away without any sign of convergence due to the lack of a stable foliation in these regimes. The region containing dots of several colors is a good approximation to the unstable manifold of the chaotic saddle. Figure 4 thus also illustrates how this manifold is evolving in time within a full period. This figure also provides us with information concerning the time evolution of the stable manifold, too, due to the symmetries mentioned above.

The shape of the structure traced out by the ensemble of droplet particles after time $t = 10\ T$ is given in Fig. 10, letting both the upper and lower half-plane and a few lobes from the tail of the chaotic saddle's unstable manifold to be seen. The resemblance to a flow visualization picture of two leapfrogging vortex rings reported in[6] is striking although the latter was obtained with three-dimensional rings in a real fluid.

4. MIXING AND TRANSPORT PROPERTIES

To understand the mixing and transport properties of the advection problem and their connection

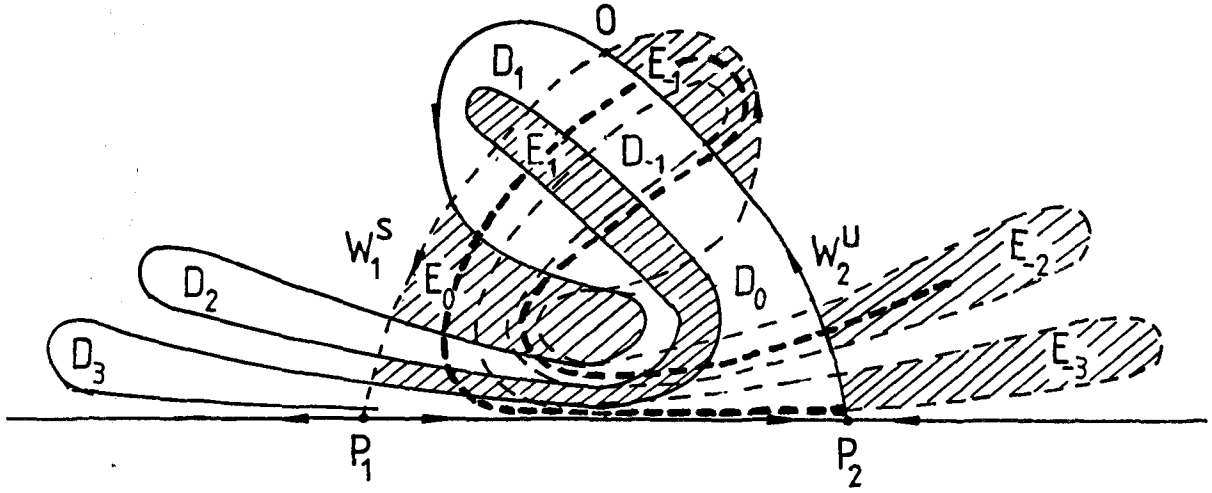

Fig. 11 Schematic diagram of the stable and unstable manifolds W_1^s and W_2^u of the fixed points P_1 and P_2, respectively, on the stroboscopic map. Note that in the full problem the invariant manifolds have other branches that can be obtained as the mirror images of W_1^s and W_2^u taken with respect to the x axis. Lobes E_i and D_i are indicated. The bold dashed line represents lobe D_{-2} whose width is comparable with the thickness of the line. In order to keep the plot clear, lobe E_{-2} is not presented.

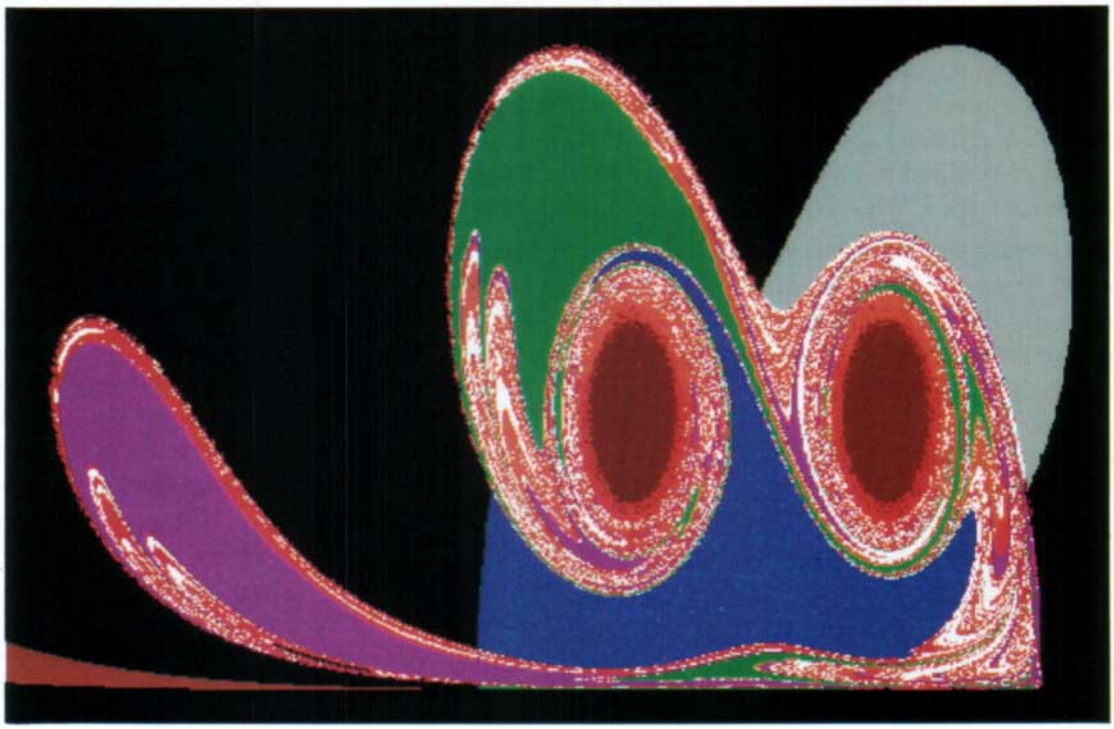

Fig. 12 Lobe dynamics. Lobe E_{-1} (gray) and its subsequent images (E_0: blue, E_1: green, E_2: magenta) are shown. The full lobe D_3 is colored by brown. The white and light red region are $E_3 \cup E_4$ and $\cup_i E_i$, $i \geq 5$ (outside of D_3), respectively. The colored region is contained in the rectangle $\{-2.9 \leq x \leq 1.2,\ 0 \leq y \leq 1.2\}$.

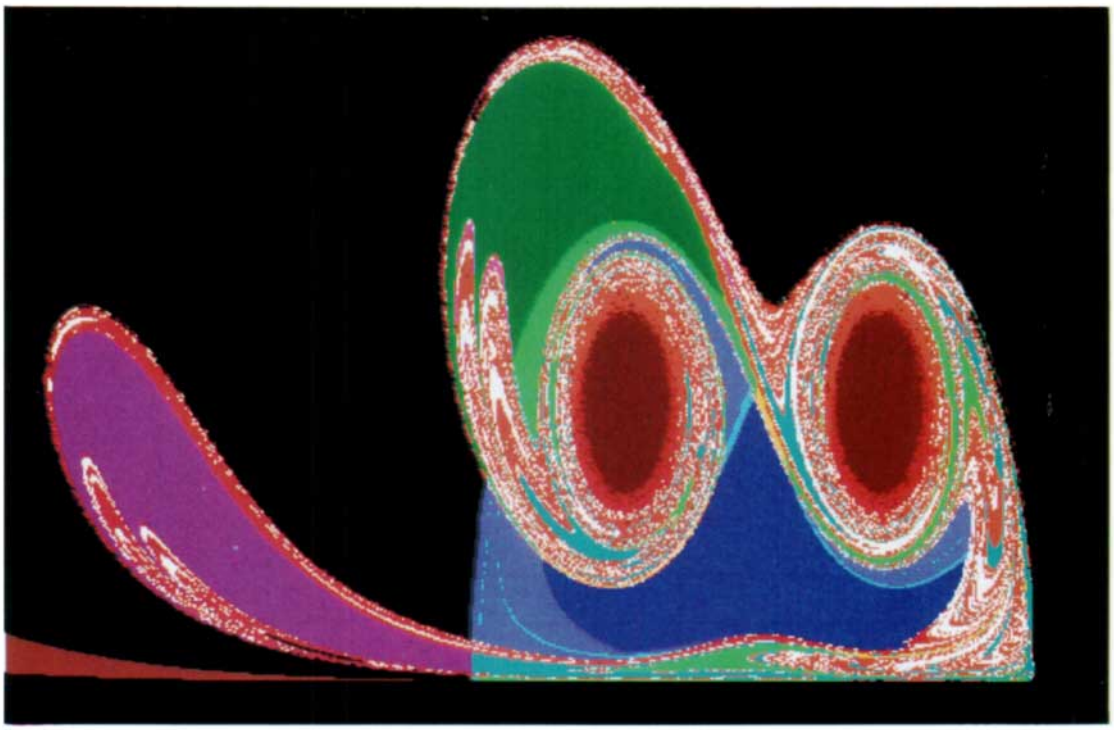

Fig. 13 Lobe dynamics subdivided according to escape. The color coding used: $E_0 \cap D_0$: dark blue, $E_0 \cap D_{-1}$: cyan, rest of E_0: light blue; $E_1 \cap D_1$: dark green, $E_1 \cap D_0$: yellow, rest of E_1: light green; $E_2 \cap D_2$: dark magenta, $E_2 \cap D_1$: light magenta, rest of E_2: light gray. The other colors are the same as in Fig. 12.

with the fractal features, it is worth studying the nontrivial manifolds of the fixed points P_1 and P_2 (denoted by W_1^s and W_2^u, respectively). If the velocity field were stationary, the stable manifold W_1^s of P_1 and the unstable manifold W_2^u of P_2 would coincide with each other and with the streamlines reaching the x-axis at these fixed points. The velocity field is, however, time-periodic and so the manifolds W_1^s and W_2^u produce several intersections.

Let us first consider the schematic Fig. 11 illustrating the most important topological features of the intersection pattern of the manifolds. One can define an *interaction region* S bounded by segment P_2O of W_2^u and segment P_1O of W_1^s, where O is the first intersection point along both manifolds. Lobes formed by the unstable manifold W_2^u and the boundary P_1O of the interaction region are denoted in the interior (exterior) of S by E_i (D_i) for $i > 0$. The tracer dynamics transforms each lobe E_i (D_i) after $t = T$ onto $E_{i+1}(D_{i+1})$. This rule extends the definition of the lobes for $i \leq 0$. We use the convention that the first (last) lobe that lies inside the interaction region has label $i = 0$. Due to the incompressibility of the flow, the area of all the lobes is equal.

It is instructive to follow how the content of a lobe is evolving, i.e., the so-called lobe dynamics.[3,14,15] One can observe that points from $E_i \cap D_j$ spend time $(i - j + 1)\ T$ inside S. In particular, points escaping the interaction region after T, independently of when they entered S, lie in D_0. Those spending just one time unit T in the interaction region lie in $E_0 \cap D_0$.

A direct numerical computation of the manifolds W_1^s and W_2^u shows that their actual form is much more complicated than those depicted in the schematic diagram. To illustrate the lobe dynamics, Fig. 12 displays the images of the material content of lobe E_{-1} (gray) after a few periods on the stroboscopic map. The compact lobe E_{-1} is mapped onto the complicated form of E_0 (blue). The next image E_1 (green) is so strongly elongated in certain regions, especially on the right side of the multicolored region, that it does not appear to be connected (although it is). This is even more pronounced in the case of E_2 (magenta) that contains all the points entering the interaction region S three periods before. The union of points that entered the interaction region 4 or 5 steps before is white. It defines a band around the unstable manifold. A good approximation to the latter is provided by the union of points that entered the interaction region more than 5 steps before (light red).

A more detailed picture of the inside of the lobes is obtained by dividing them according to the time of *escaping* the interaction region. In Fig. 13 we divide lobe E_0 into subregions escaping after one, two or more steps, and indicate the images of these subregions. Points from lobe E_0 that escape immediately (i.e., points of $E_0 \cap D_0$, dark blue) are after one and two steps in $E_1 \cap D_1$ (dark green) and $E_2 \cap D_2$ (dark magenta), respectively. The boundary between dark and light green and dark magenta and gray traces out — by definition — pieces of the outermost branch of the stable manifold. It is worth noting that points of E_0 escaping after one step ($E_0 \cap D_{-1}$, cyan) form a rather narrow filament. In contrast to the schematic Fig. 11, D_{-1} has 24 intersection points with E_0. Because of the very strong stretching, the cyan domain is in certain regions quite close to the internal branches of the saddle's stable manifold. Its first and second images are coded by yellow and light magenta. They can be seen around the midpoint between the vortices and at the tips of the two internal white-red tongues inside D_1, respectively. Points of the light blue region close to the cyan filament can, however, stay for a very long time in the interaction region.

These observation indicate that the set $E_0 \cap D_{-n}$ ($D_0 \cap E_n$), or more generally, $E_i \cap D_{-n}$ ($D_i \cap E_n$), provide with $n \to \infty$ and i fixed an ever refining approach to the stable (unstable) manifold of the chaotic saddle inside the interaction region.

5. MULTIFRACTAL ANALYSIS

Tracer particles injected into the fluid in front of the leapfrogging vortices exhibit, with the exception of a set of initial conditions of measure zero, an asymptotically simple motion, with a complicated, chaotic part restricted to a finite domain in both space and time. The particle motion is thus analogous to a *scattering* process that is chaotic in the region of strong interaction. Recent developments in the field of *chaotic scattering*[16] can thus be taken over and used to characterize fractal and multifractal properties of the tracer dynamics.

A central object in the theory of chaotic scattering is the *time delay function* describing how the time spent in the interaction region depends on the initial conditions. In practice, one takes a one-parameter family of initial conditions (say a straight line on the (x, y) plane) and measures the

number of periods the particle needs to leave a preselected region around the vortices as a function of the parameter. In our numerical experiment $5 \cdot 10^4$ trajectories were started with uniform distribution on a vertical segment of length 0.1 at $x = 1.3$ cutting through the lobe E_{-2}. We then measured after how many time periods of T they crossed the vertical line at $x = -1.3$, and thus left the vortices. This function depicted in Fig. 14 takes on an infinite value whenever the initial condition falls on the stable manifold of the chaotic saddle. These infinities thus appear in a fractal pattern. The set of infinities is a kind of projection of the Cantor set $\mathcal{C}_u$ along the stable manifold (see Fig. 5). The former has thus the same dimension d_0 as the dimension of the Cantor set $\mathcal{C}_u$.

Trajectories characterized by different time delay values mark different levels in a *hierarchy*. We define on each level n length scales $l_i^{(n)}$ that denote the length of intervals where the time delay function takes on a value greater than or equal to nT (the first two levels are indicated at the bottom of Fig. 14). The set of intervals at level n is practically the cross-section of the complement of lobes $D_{-2}, D_{-3}, \ldots, D_{-n}$ inside E_{-2} with the $x = 1.3$ line. This is so because the lifetime of particles in $E_i \cap D_j$ is $(i - j + 1)T$ inside S. Thus we conclude that the hierarchy seen in the time delay function also reflects the hierarchy of the lobes D_j with $j < 0$. The relation between these hierarchies follows from our previous observation claiming that $E_{-i} \cap D_{-n}$ approaches to the stable manifold for increasing n.

The set of intervals taken represents a refining coverage of the singularities in the time delay function, i.e., of a fractal set of dimension d_0. Let the total number of such intervals at level n be denoted by $N(n)$. It is usually an exponentially increasing function of n in the large n limit. The total interval length, however, decreases with n,

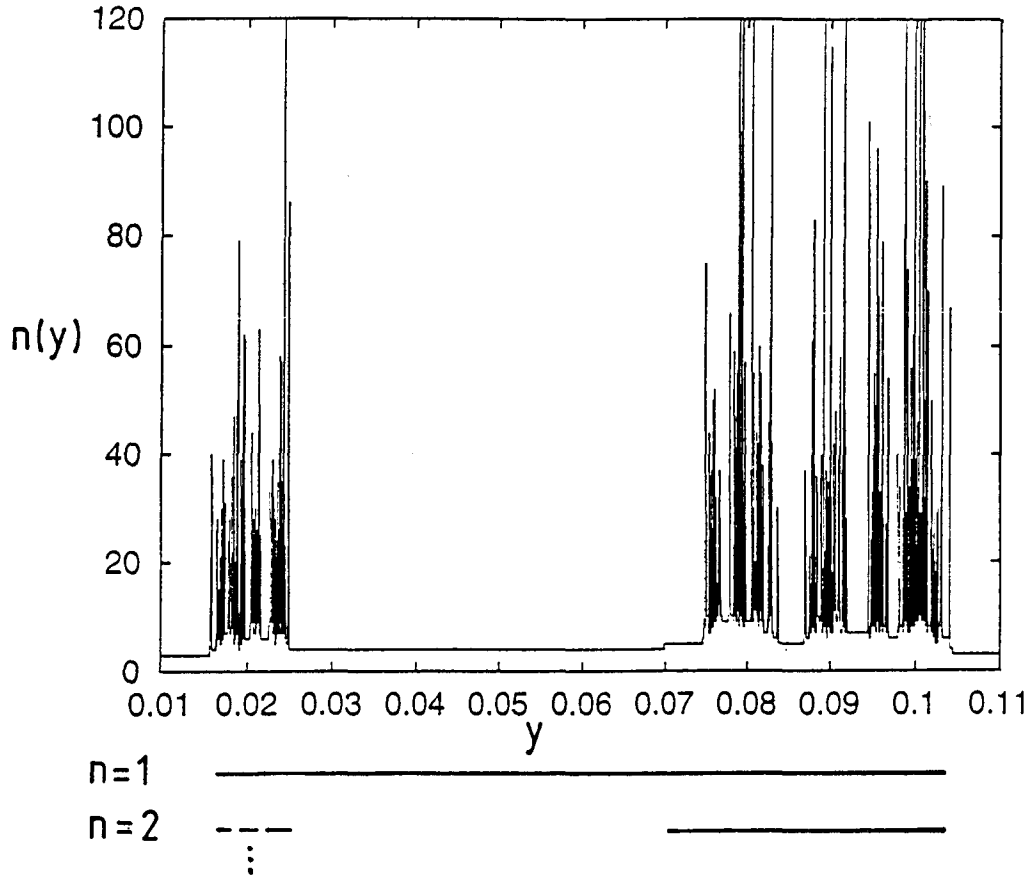

Fig. 14 Time delay function. $5 \cdot 10^4$ trajectories were started on the $x = 1.3$ line with $0.01 < y < 0.11$. The first two levels in the hierarchical organization are also shown, that are practically the crossections of the $x = 1.3$ line with E_{-2} and $E_{-2} \backslash D_{-2}$, respectively (cf. Fig. 11). The intervals on the nth level would correspond to $E_{-2} \backslash (\cup_{i=-2}^{-n} D_i)$.

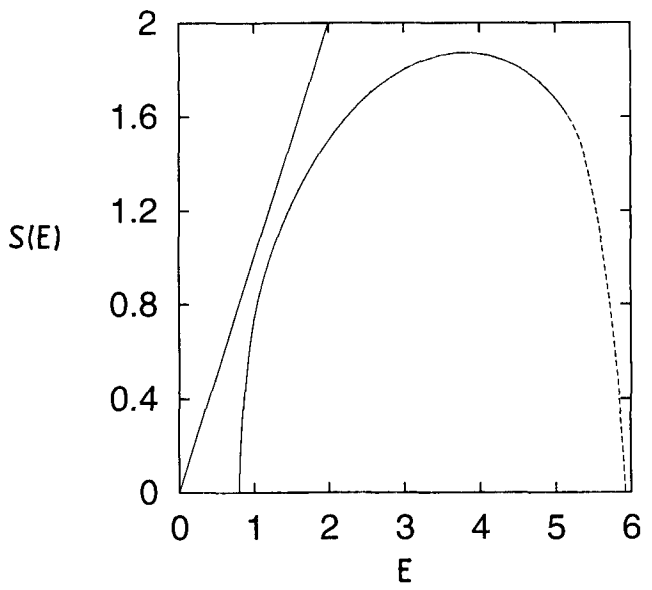

(a)

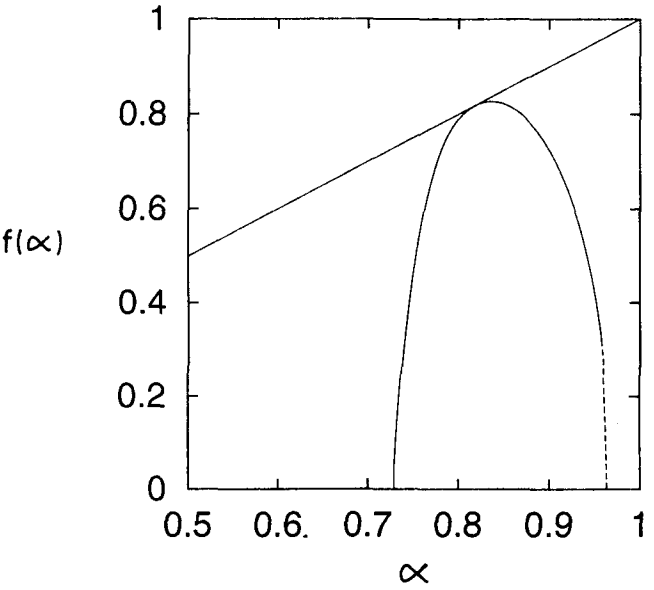

(b)

Fig. 15 The entropy function $S(E)$ of the local Lyapunov exponents of the chaotic saddle's hyperbolic component extracted from the coverage of the singularities in the time delay function of Fig. 14 via Eq. (4) (a), and the corresponding $f(\alpha)$ spectrum (*b*). The straight lines represent the diagonals. The support of the entropy function and the $f(\alpha)$ function is $E_- = 0.80 \leq E \leq E_+ = 5.92$ and $\alpha_- = 0.73 \leq \alpha \leq \alpha_+ = 0.96$, respectively. Considerable numerical uncertainties are due to the difficulty of an accurate determination of the rapidly shrinking intervals. Such regions are plotted by dashed lines.

$\sum_{i=1}^{N(n)} l_i^{(n)} \sim \exp(-\gamma n)$ where γ is called the escape rate.

Having found a hierarchically nested set of characteristics, we can carry out a multifractal type analysis of the length scale statistics in the same spirit as for any fractal with a hierarchical organization.[17] We introduce scaling indices E by writing:

$$E_i = -\frac{1}{n} \ln l_i^{(n)} . \tag{2}$$

They tell us how rapidly the length scales decrease with n and can be considered as local *Lyapunov exponents*. The range in which the values E_i lie is typically a finite interval (E_-, E_+).

As n grows, there are in the coverage more and more intervals of the same exponent E. Their number $W(n, E)$ also grows exponentially, and we can define an entropy function $S(E)$ of the local Lyapunov exponents as the growth rate of W:

$$W(n, E) \sim e^{S(E)n} , \tag{3}$$

valid for large n. Alternatively, it can be obtained as the Legendre transform of the so-called free energy $\beta F(\beta)$, extracted from a weighted sum of the length scales via the relation:

$$\sum_{i}^{N(n)} (l_i^{(n)})^{\beta} \sim e^{-\beta F(\beta) n}, \tag{4}$$

where β is an arbitrary real number, and $n \gg 1$.

The function $S(E)$ characterizes the length scale distribution of the intervals covering the singularities in the time delay function. These intervals are transported away by the flow along the stable manifold, are slightly deformed, and come after a certain time close to the Cantor set C_u. The Cantor set's coverage has thus the same scaling properties as the intervals in the time delay function. Therefore, the same entropy function $S(E)$ characterizes the chaotic saddle, too.[18] The entropy function of local Lyapunov exponents for the tracer dynamics obtained from the time delay function of Fig. 14 is displayed in Fig. 15(a).

Local Lyapunov exponents can also be determined directly by following the deformation of material lines.[19] Our approach based on the analogy with chaotic scattering seems to be simpler than previous ones since it requires the analysis of only straight line segments on an interval.

One can prove[17,18] that the value of E that belongs to the point with slope unity of $S(E)$ is the

average Lyapunov exponent λ of the dynamics. The horizontal distance of this point from the diagonal $S = E$ is the escape rate γ. The dimension d_0 can be read off as the slope of the straight line passing through the origin and being tangent to the graph of $S(E)$. In our problem we obtain for the fractal dimension, the average Lyapunov exponent, and the escape rate the values $d_0 = 0.83$, $\lambda = 1.18$ and $\gamma = 0.22$, respectively. Notice that the range of local Lyapunov exponents is rather broad.

One can define a natural distribution on the chaotic saddle describing how often different pieces of the set are visited by trajectories staying for a long time around it. It turns out that the measure of a box taken with respect to this natural distribution is proportional to its linear size. The natural measure of the set is thus a geometrical multifractal.[20] More precisely, the measure of each interval covering the Cantor set $\mathcal{C}_s$ or $\mathcal{C}_u$ is proportional to the length of the interval. Normalization implies that $e^{\gamma} l_i^{(n)}$ can be considered as the interval measure. It is easy to see then that the $f(\alpha)$ spectrum[21] taken with respect to this measure can be expressed entirely by the Lyapunov spectrum $S(E)$ as[17]:

$$f(\alpha) = \left.\frac{S(E)}{E}\right|_{E=\gamma/(1-\alpha)} . \tag{5}$$

The graph of this multifractal spectrum is plotted in Fig. 15(b).

Time reversal invariance also implies that the Cantor sets $\mathcal{C}_s$ and $\mathcal{C}_u$, the building blocks of the hyperbolic component, have identical multifractal properties. Consequently, if d_q denotes the generalized dimension[22] of one Cantor set computed from Eq. (5), $2d_q$ is the order q dimension of the full chaotic saddle's hyperbolic component.

The considerations above show that the fractal patterns in chaotic advection are examples where the underlying dynamics uniquely determines the fractal properties. By taking the derivative of expression (5) with respect to α at $\alpha_1 \equiv d_1$, where the slope of f is unity, we recover a basic relation[23]:

$$d_1 = 1 - \gamma/\lambda . \tag{6}$$

It says that the deviation of the information dimension from unity is a ratio of numbers measuring the global repulsion (γ) and the local instability (λ). Sets repelling stronger are more rarified and have smaller information dimensions (provided their λ is the same). In our example $d_1 = 0.815$. Relation (6) is again a nice example of how the chaotic dynamics determines fractality.

6. SUMMARY AND DISCUSSION OF EXPERIMENTAL IMPLICATIONS

The general observations of this paper are obviously valid for any two-dimensional time-periodic incompressible flow that is asymptotically simple.[24–26] By the latter we mean that the time dependence of the velocity field is restricted to a central region, and further away upstream or downstream the velocity is practically stationary. In such cases tracer trajectories can be unbounded, and, because of the asymptotic simplicity of the motion, the particle dynamics can be considered as a type of scattering process. If the tracer dynamics is chaotic, this type of chaos is unavoidably of a transient type, i.e., restricted to finite times scales. The key observation in understanding the phenomenon is the existence of an *invariant chaotic saddle* in the flow. This invariant set is globally nonattracting and cannot be reached exactly. The chaotic saddle is itself a fractal with a local structure resembling the direct product of two Cantor sets in certain regions.

A chaotic saddle also has a stable manifold, a curve along which the set can be reached, an object of *measure zero* that provides a fractal foliation of the space. This is why a particle has zero probability to be trapped forever by the chaotic saddle. Analogously, the set also has an *unstable manifold* that is fractal, too.

Fractal patterns observed in the tracer dynamics can be attributed to the double foliation of the space by the two manifolds. An adequate characterization of the advection requires the study of an *ensemble* (droplet or line segment) of tracers. If the initial points of some the tracer trajectories lie close to one branch of the unstable manifold, particles will approach the chaotic saddle along this branch, stay a long time around the set, and finally escape along its unstable manifold. Thus, dye particles not advected away very quickly to the asymptotic region accumulate on the unstable manifold of the chaotic saddle. We conclude that a fractal pattern can always be found if the tracer dynamics of the flow is chaotic and the set of initial conditions used happens to overlap with the stable manifold of the chaotic saddle (see also Refs. 4, 14, 24, 26 and 27). This is an extension of results obtained in closed flows[28,29,30] claiming that dye particles move asymptotically along unstable manifolds of periodic orbits embedded in the chaotic sea. We pointed out that fractal and multifractal properties can easily be

derived by studying the singularity structure of the time delay function, a basic characteristics of the scattering tracer dynamics.

Our findings make even in a *laboratory experiment*, the determination of the chaotic saddle and its invariant manifolds, possible. Inject a droplet into the flow in front of the central region where the velocity field is strongly time-dependent. Dye particles that have not yet escaped this region after several periods trace out the unstable manifold. By means of modern video technique,[31] the stable manifold can also be obtained. It contains points that approach the chaotic saddle and stay there forever. Since the manifold is a set of measure zero, such points are unlikely to be found. One can, however, locate narrow bands surrounding the branches of this manifold that contain points staying around the chaotic saddle for a long time before escaping. In particular, by taking a video record of several such tracer trajectories, their initial points provide a good approximation to the stable manifold.

The chaotic saddle itself can also be located in a laboratory experiment by means of the so-called ensemble or sprinkler method.[23,32,9] One distributes a large number of particles in a preselected region around the chaotic saddle and follows their motion. Only particles staying in this region for a long time are considered. Their trajectories contain sections describing the approach to and the escape from the chaotic saddle; therefore, these sections have to be discarded. The trajectories truncated in this way characterize the motion on a close neighborhood of the chaotic saddle.

These methods can be comprised in one single approach. Set a critical number n_0 of periods and take a record of several trajectories that escape the central region of the flow in a time period longer than n_0. The initial and final points of such trajectories, and the ones in the middle, trace out the stable and unstable manifolds, and the chaotic saddle, respectively, with an accuracy increasing with n_0.[33] The statistics can be improved by overlapping points obtained at different values of n_0. To illustrate this method, we plotted in Fig. 16 points that escape the interaction region in the field of the leapfrogging vortex pairs later than 5 periods in *both* the direct and the time reversed dynamics. These are points that belong simultaneously to both the stable and unstable manifold specified with a finite resolution. This corresponds to levels $n > n_0/2 = 5$ of the hierarchy defined by the lobe dynamics or the time delay function. A comparison

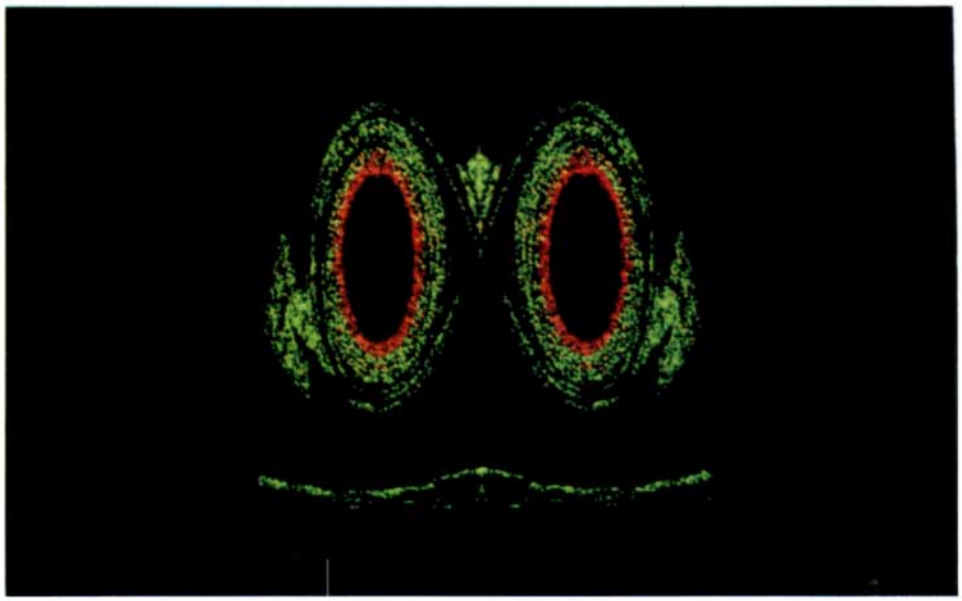

Fig. 16 Chaotic set plotted by recording points which stay longer than a given number of steps within the scattering region both in the forward and backward dynamics. The union of sets $E_i \cap D_{-j}$, $5 < i, j \leq 13$ is shown in yellow. Tracers with a life-time longer than 13 in both the direct and time reversed dynamics are colored by red and mark the nonhyperbolic part of the chaotic saddle. The colored region is contained in the rectangle $\{|x| \leq 1.114, 0 \leq y \leq 0.81\}$.

with Fig. 6(a) shows that the resolution is nearly as good as the one obtained there but the present visualization of the saddle can in principle be carried out in laboratory experiments, too.

ACKNOWLEDGMENTS

One of us (T. T.) is deeply indebted to L. Sasvári for introducing him to the problem of vortex dynamics. Valuable discussions with S. Jones, G. Károlyi, Z. Kovács, O. Piro, A. Provenzale, L. Sasvári and L. Zannetti are acknowledged. This work was partially supported by the Hungarian Science Foundation under Grant Nos. OTKA 2090, T4439, F4286; by the Foundation for Hungarian Higher Education and Research; and by the PHARE ACCORD program H9112-0378.

REFERENCES

1. J. M. Ottino, *The Kinematics of Mixing: Stretching, Chaos and Transport* (Cambridge University Press, Cambridge, 1989); J. M. Ottino, *Ann. Rev. Fluid. Mech.* **22**, 207 (1990); J. M. Ottino, S. C. Jana and V. S. Chakravarthy, *Phys. Fluids* **6**, 685 (1994); S. C. Jana, G. Metcalfe and J. M. Ottino, *J. Fluid Mech* **269**, 199 (1994).
2. A. Crisanti, et al. *La Rivista del Nuovo Cimento* **14**, 1 (1991).
3. S. Wiggins, *Chaotic Transport in Dynamical Systems* (Springer, 1992).
4. K. Shariff et al. *Fluid. Dyn. Res.* **3**, 337 (1988).
5. K. Shariff and A. Leonard, *Ann. Rev. Fluid. Mech.* **24**, 235 (1992); K. Shariff, PhD Thesis, Stanford University, 1989.
6. H. Yamada and T. Matsui, *Phys. Fluids* **21**, 292 (1978). M. Van Dyke, *An Album of Fluid Motion* (The Parabolic Press, Stanford, 1982), p. 46.
7. K. B. Shoutherland et al. *Phys. Fluids* **A3**, 1385 (1991); G. J. F. van Heijst and J. B. Flór, *Nature* **340**, 212 (1989); G. F. Carnevale, R. C. Kloosterziel and G. J. F. van Heijst, *J. Fluid. Mech.* **233**, 119 (1991); D. Auerbach, *Phys. Fluids* **A3**, (1991), 1351.
8. Á. Péntek, T. Tél and Z. Toroczkai, *Chaotic Advection in the Velocity Field of Leapfrogging Vortex Pairs, J. Phys. A* (in press).
9. T. Tél, In: *Directions in Chaos*, Vol. 3, ed. Hao Bai-Lin (World Scientific, Singapore, 1990) pp. 149–221.
10. P. G. Saffman, *Vortex Dynamics* (Cambridge Univ. Press, Cambridge, 1992); H. Aref, *Ann. Rev. Fluid. Mech.* **15**, 345 (1983); V. V. Meleshko et al., *Phys. Fluids* **A4**, 2779 (1992); V. V. Meleshko and G. J. F. Van Heijst, *Chaos, Solitions and Fractals* **7**, 977 (1994).
11. J. Guckenheimer and P. Holmes, *Nonlinear Oscillations, Dynamical Systems, and Bifurcations of Vector Fields* (Springer, Berlin, 1983).
12. H. E. Nusse and J. Yorke, *Physica* **D36**, 137 (1989).
13. Y. T. Lau, J. M. Finn and E. Ott, *Phys. Rev. Lett.* **66**, 978 (1991).
14. V. Rom-Kedar, A. Leonard and S. Wiggins, *J. Fluid. Mech.* **214**, 347 (1990).
15. D. Beigie, A. Leonard and S. Wiggins, *Phys. Fluids* **A3**, 1039 (1991); R. Camassa and S. Wiggins, *Phys. Rev.* **A43**, 774 (1991); J. B. Weiss and E. Knobloch, *Phys. Rev.* **A40**, 2579 (1989).
16. E. Ott and T. Tél, *Chaos* **3**, 417 (1993).
17. T. Tél, Z. *Naturforsch.* **43a**, 1154 (1988).
18. Z. Kovács and T. Tél, *Phys. Rev. Lett.* **64**, 1617 (1990).
19. A. Vulpiani, *Physica* **D38**, 372 (1989); F. Városi, T. M. Antonsen, Jr. and E. Ott, *Phys. Fluids* **A3**, 1017 (1991); D. Beigie, A. Leonard and S. Wiggins, *Phys. Rev. Lett.* **70**, 275 (1993); S. Gallucio and A. Vulpiani, *Physica A* **212**, 75 (1994).
20. T. Tél and T. Vicsek, *J. Phys.* **A20**, L835 (1987).
21. T. C. Halsey et al., *Phys. Rev.* **A33**, 1141 (1986).
22. P. Grassberger and I. Procaccia, *Physica* **D13**, 34 (1984).
23. H. Kantz and P. Grassberger, *Physica* **D17**, 75 (1985)
24. K. Shariff, T. H. Pulliam and J. M. Ottino, *Lect. Appl. Math.* **28**, 613 (1991).
25. C. Jung and E. Ziemniak, *J. Phys* **A25**, 3929 (1992); C. Jung, T. Tél and E. Ziemniak, *Chaos* **3**, 555 (1993).
26. E. Ziemniak, C. Jung and T. Tél, *Physica* **D76**, 123 (1994); C. Jung and E. Ziemniak, in: *Fractals in the Natural and Applied Sciences*, M. M. Novak et al., (North Holland, Amsterdam, 1994).
27. Á. Péntek, et al., *Fractal boundaries in open hydrodynamical flows: signatures of chaotic saddles, Phys. Rev. E* (in press).
28. H. Aref and S. Balachandar, *Phys. Fluids* **29**, 3515 (1986).
29. J. Chaiken, et al., *Proc. Roy. Soc. Lond.* **A408**, 154 (1986).
30. F. J. Muzzio, P. D. Swanson and J. M. Ottino, *Int. J. Bifurc. Chaos* **2**, 37 (1992).
31. T. H. Solomon, E. R. Weeks and H. L. Swinney, *Phys. Rev. Lett.* **71**, 3975 (1993); *Physica* **D76**, 70 (1994); J. C. Sommerer and E. Ott, *Science* **259**, 281 (1993); J. C. Sommerer, *Physica* **D76**, 85 (1994).
32. G. H. Hsu, E. Ott, and C. Grebogi, *Phys. Lett.* **A127**, 199 (1988).
33. Y. Lai, T. Tél and C. Grebogi, *Phys. Rev.* **E46**, 709 (1993).

APPENDIX: ADVECTION BY LEAPFROGGING VORTEX PAIRS

The dynamics of point vortices in two-dimensional flows is a classical field of research in hydrodynamics.[10] The equations of motion of a system of such vortices in an ideal incompressible fluid can be cast into a canonical form by introducing a Hamiltonian that in suitably chosen units reads as:

$$H(\{x_i, y_i\}) = -\sum_{i<j} \kappa_i \kappa_j \ln r_{i,j} \,. \tag{7}$$

Here (x_i, y_i) stands for the position of vortex $i (i = 1, \ldots, n)$ in the (x, y) plane, $r_{i,j}$ is the distance between vortices i and j, and κ_i denotes the dimensionless vortex strengths. The value E_0 of the Hamiltonian is constant in time and can thus be called the energy of the vortex system. The equations of motion of vortices is of Hamiltonian type[10]:

$$\kappa_i \dot{x}_i = \frac{\partial H}{\partial y_i}, \quad \kappa_i \dot{y}_i = -\frac{\partial H}{\partial x_i} \,. \tag{8}$$

Note the analogy with the canonical equations of point mechanics when one identifies, for example, x and κy with the generalized coordinates and momenta, respectively. We consider the motion of two vortex pairs of equal strengths ($\kappa_1 = \kappa_2 = -\kappa_3 = -\kappa_4 \equiv 1$) that move in the same direction along a common symmetry axis perpendicular to the extension of both pairs ($x_1 = x_4$, $y_1 = -y_4$, $x_2 = x_3$, $y_2 = -y_3$) as depicted in Fig. 1. It follows from the conservation of the momentum (y-coordinates) that $y_1 + y_2$ is a constant and we shall take this quantity as the length unit in the calculations. It is worth using a frame comoving with the center of mass of the upper two vortices $x_0 \equiv (x_1 + x_2)/2$. Note that the velocity $\dot{x}_0$ of the center of mass is now *not* constant (Eq. (11)). The equations of motion for the relative coordinates x_r, y_r are obtained as[8]:

$$\dot{x}_r = -2y_r \frac{1 + x_r^2}{(1 - y_r^2)(x_r^2 + y_r^2)} \,, \tag{9}$$

$$\dot{y}_r = 2x_r \frac{1 - y_r^2}{(1 + x_r^2)(x_r^2 + y_r^2)} \,. \tag{10}$$

They are decoupled from the center of mass dynamics:

$$\dot{x}_0 = \frac{x_r^2 - y_r^2 + 2}{(1 - y_r^2)(1 + x_r^2)} \,. \tag{11}$$

It is easy to check that the vortices undergo a strictly periodic motion, i.e., they are leapfrogging, if the energy E_0 of the vortex system is positive. In this paper we have fixed the energy value to $E_0 = \ln 2$ that corresponds to loosely bounded vortex pairs. The period of the vortex motion is then $2\,T = 2.16$ in dimensionless units.

The streamfunction $\psi(x, y)$, whose cross derivatives yield the velocity components v_x, v_y[10] (cf. Eq. (13)), is $-\kappa \ln r$. In the system of n vortices these contributions are superimposed, and one obtains:

$$\psi(x, y, t) = -\sum_j \kappa_j \ln r_j(t) \,, \tag{12}$$

where $r_j(t)$ stands for the distance of point (x, y) from vortex j. The vortices follow their own dynamics, thus the distances $r_j(t)$, and consequently also the streamfunction, are time-dependent. The velocity components at a given point (x, y) and time t are then obtained as:

$$v_x(x, y, t) = \frac{\partial \psi}{\partial y}, \quad v_y(x, y, t) = -\frac{\partial \psi}{\partial x} \,. \tag{13}$$

Because of the interchangeability of the vortex pairs ($\kappa_1 = \kappa_2$), the velocity field is of period T if the leapfrogging motion has period $2\,T$.

A passively advected particle simply follows the local velocity field; therefore, its equations of motion are given by:

$$\dot{x} = \frac{\partial \psi(x, y, t)}{\partial y}, \quad \dot{y} = -\frac{\partial \psi(x, y, t)}{\partial x} \,. \tag{14}$$

Note again the canonical character of the problem in which the streamfunction plays the role of the Hamiltonian.

In the reference frame used whose origin is comoving with the point $(x_0(t), 0)$ along the x-axis (the Center of Mass System) the streamfunction is:

$$\psi_{CMS}(x, y, t) = \psi(x, y, t) - \dot{x}_0(t) y \,. \tag{15}$$

The difference when compared with the vortex dynamics is that the problem is now nonautonomous and it is the motion of the vortex centers that brings about the time dependence, and leads to chaotic time evolution of tracer particles.